Helium cluster dissolution in molybdenum

2009 J. Phys.: Condens. Matter 21 335401

(http://iopscience.iop.org/0953-8984/21/33/335401)

J. Phys.: Condens. Matter **21** (2009) 335401 (6pp) doi:10.1088/0953-8984/21/33/335401

Helium cluster dissolution in molybdenum

O Runevall and N Sandberg

Department of Physics, Royal Institute of Technology, S-106 91 Stockholm, Sweden

E-mail: odd@neutron.kth.se and nils@neutron.kth.se

Received 17 March 2009, in final form 3 June 2009
Published 24 July 2009
Online at stacks.iop.org/JPhysCM/21/335401

Abstract

Helium retention and diffusion in molybdenum is studied on an atomistic scale with *ab initio* methods. The thermal stability of helium–vacancy clusters is quantified within the framework of density functional theory. Calculated helium emission rates are used to derive a desorption spectrum which is compared with experimental results. The agreement between the current calculations and available experiments is satisfactory except in the high temperature end of the spectrum. The current results indicate that above 1100 K He migration is assisted by lattice defects such as vacancies, rather than through interstitial diffusion.

1. Introduction

In nuclear reactor materials, helium may be introduced by nuclear reactions. Due to the high heat of solution of helium in metals it will agglomerate into clusters and diffuse to dislocations and grain boundaries [1]. This has important consequences for material properties like, for example, ductility. Modelling of helium in metals is well established within the framework of density functional theory (DFT) [2–10]. However, even though these studies give essential results for an atomistic description of helium clustering in metals, most of them do not give sufficient data for kinetic modelling needed to fully compare the results with experimental data.

The purpose of this paper is to model the dissolution of helium clusters in molybdenum, as measured in desorption experiments [11, 12]. Our modelling is based on standard DFT calculations providing (i) static information on the structure of helium clusters and on helium emission activation energies and (ii) dynamic information on relative vibrational frequencies, which contribute to the prefactors of the helium emission rates. Taken together, this gives information on absolute helium emission rates from clusters of various sizes, which are in turn used as input in a rate-theory model of helium cluster desorption spectra. We choose to study molybdenum due to the existence of well-controlled experiments performed on single crystals [13, 11, 12]. Thus, in the modelling of helium desorption, we regard molybdenum as being representative for the class of bcc metals, and we briefly discuss the implications of the current findings for the iron–helium system at the end of this paper.

2. Theoretical background

Most quantitative data on helium retention and diffusion in metals is based on desorption experiments. In such an experiment helium release rates from a single crystal injected with helium is observed while the crystal is being heated at a constant heating rate. In the crystal, the helium can be assumed to cluster in molybdenum vacancy positions. Here, these clusters are denoted $\mathrm{He}_n\mathrm{V}_m$. Under controlled experimental conditions one can assume the following state evolution for these clusters [13, 12]:

$$\mathrm{He}_n\mathrm{V} \rightarrow \mathrm{He} + \mathrm{He}_{n-1}\mathrm{V} \qquad n > 1 \tag{1}$$

$$\mathrm{He}_1\mathrm{V} \rightarrow \mathrm{He} + \mathrm{V} \qquad n = 1 \tag{2}$$

where He represents an interstitial helium atom and V a vacancy. Clusters with more than one vacancy have in this model been disregarded due to experimental conditions, which will be discussed in more detail later. Interstitial helium atoms are assumed to diffuse to the boundary of the crystal and from there to be released to the surroundings. No recapturing of interstitial helium in clusters is assumed due to the rather high heating rate used in experimental work.

For this model the jump rate in between states can be written [14] as

$$\Gamma = \nu^* \mathrm{e}^{-\Delta F/k_\mathrm{B}T} \tag{3}$$

where ν^* is an effective frequency associated with the vibration of the helium atom, ΔF the free energy change associated with the jump of a helium atom from a substitutional to an interstitial position, k_B the Boltzmann constant and T the absolute temperature. However, ν^* cannot be directly assessed from experimental data. Therefore another frequency, $\tilde{\nu}$, has

to be introduced by expressing the free energy change in terms of the change in internal energy, ΔE, and the entropy change, ΔS, by $\Delta F = \Delta E - T\Delta S$:

$$\Gamma = \nu^* e^{\Delta S/k_B} e^{-\Delta E/k_B T} = \tilde{\nu} e^{-\Delta E/k_B T}. \quad (4)$$

For the state evolution in (1) and (2) ΔE can also be interpreted as the binding energy of a helium atom to the helium–vacancy cluster. With the state evolution of (1) and (2) and the jump rate Γ, a set of ordinary differential equations (ODE) can be formulated:

$$\frac{dn_i}{dt} = \Gamma_{i+1} - \Gamma_i \quad (5)$$

with n_i as number of helium–vacancy clusters containing i helium atoms and Γ_i as the jump rate from a cluster with i helium atoms to a cluster with $i-1$ atoms.

From *ab initio* calculations ν^* can be assessed directly. It is here evaluated by applying the theory of harmonic lattice vibrations [15], from which the vibrational spectra ω for helium atom vibrations in the cluster configurations were calculated. In this work ν^* was then taken as $\nu^* = \max(\omega)$.

3. Calculation methods

The current DFT calculations are based on the Vienna *ab initio* simulation package (VASP) [16–18] and all calculations were performed on a supercell containing $4 \times 4 \times 4$ bcc unit cells with a k-point mesh of $3 \times 3 \times 3$ points and a cutoff energy of 500 eV. All calculations were performed using the PAW general gradient approximation (GGA) potentials supplied by the VASP group [18]. Due to the nonmagnetic nature of molybdenum nonspin polarized settings were used. The cell size, k-point density and cutoff energy were selected after convergence tests on a bulk system, a vacancy state and a He_1V_1 cluster, respectively. The convergence with respect to cell size is crucial in these calculations, mainly since periodic boundary conditions are implemented in VASP. The convergence of the total energy in the calculations due to cell size is affected both by electronic forces and elastic forces in the crystal. The electronic forces converge as $O(L^{-5})$ [19], with L as the cell size, and since the three test cases are converged regarding this, cells containing larger numbers of helium atoms should be converged as well. The convergence of the elastic forces is discussed later.

The absolute energy E of each helium–vacancy cluster was calculated, and from that the formation energy ΔE_f from

$$\Delta E_f = E - N_{Mo} E(\text{Mo}) - N_{He} E(\text{He}) \quad (6)$$

where N_{Mo} and N_{He} are the number of molybdenum and helium atoms in the cell, respectively, and $E(\text{Mo})$ and $E(\text{He})$ are the absolute energy per atom of bulk molybdenum and a free helium atom, respectively. From the formation energies the binding energy of helium atoms to each helium–vacancy cluster were calculated in line with reactions (1) and (2). ν^* was calculated as described above for each helium–vacancy cluster and the interstitial sites. These calculations were performed by displacing each atom in steps of 0.02 Å twice in each direction, calculating the forces acting on all atoms and from that deriving ω.

To calculate $\tilde{\nu}$ from ν^* entropy contributions were added. Two such contributions were accounted for, first the configurational contribution from symmetry degeneration due to the number of ways to orient each cluster in the vacancy and, second, that due to changes in the vibrational spectra. The former was calculated from

$$\Delta S = S_{He} + S_{He_{n-1}V_1} - S_{He_nV_1} = k_B \ln \frac{W_{He} W_{He_{n-1}V_1}}{W_{He_nV_1}} \quad (7)$$

with W as the number of possible configurations for each state lattice atom. To ensure a relaxation of the helium atoms in each supercell into the most energetically favourable positions, the atoms were placed in such a way that the symmetry of the cell was minimized (corresponding to a large W value) and then allowed to relax into a more symmetric state. There is a possibility, especially for the clusters with larger numbers of helium atoms, that there exist several configurations minimizing the total energy. However, our approach does not take this into account. The contribution from changes in vibrational spectra was taken as the ratio of the maximal frequency of the interstitial state and the initial state in line with the discussion of Vineyard [14].

The calculated binding energies and $\tilde{\nu}$, gave a set of jump rates $\{\Gamma_i\}_{i=1}^5$ for helium–vacancy clusters containing up to five helium atoms. With these a system of ODEs were formulated in accordance with (5). This system was, due to its nonlinearity, solved numerically by the forward Euler method.

4. Results

The formation energy of the vacancy state, the di-vacancy cluster and the two highly symmetric and possibly stable interstitial (octahedral and tetrahedral) states were calculated and are found in table 2. As seen, the tetrahedral position is the thermodynamically stable of the two. In fact, after calculating the migration path in between tetrahedral states, with activation energy of 0.053 eV, it was concluded that helium migrates in between tetrahedral states without passing through any octahedral state, and that the diffusion is close to athermal, and was therefore considered immediate in the modelling efforts. These results are qualitatively similar to those for helium in α-iron calculated by Fu and Willaime [2]. In table 2 it is also seen that the calculated vacancy formation energy is somewhat lower than the experimentally determined one, which is due to the performance of the exchange correlation function in DFT in this type of system, as discussed by several authors [20, 21]. This could be solved by adding a correction, but so has not been done in this work since the effect cancels in most cases when the binding energy is calculated.

It is of importance for the calculation of $\tilde{\nu}$ to discuss the symmetry break of the lattice due to helium–vacancy clusters since this affects the entropy, as seen from equation (7). Figures 1 and 2 visualize the equilibrium positions of helium atoms in the clusters and W as determined from symmetry considerations of these positions can be found in table 1. As shown in these figures the helium atom in the He_1V_1 cluster

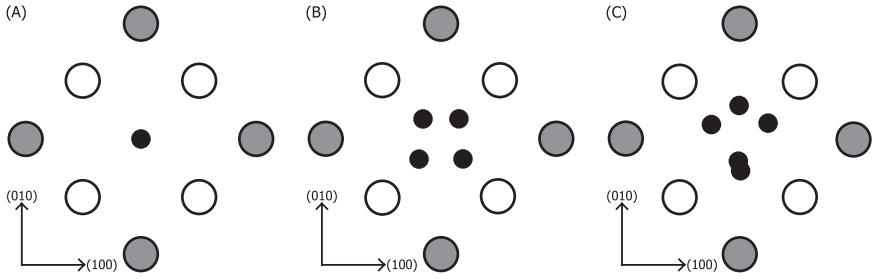

Figure 1. Projection of helium–vacancy clusters and twelve neighbouring molybdenum atoms into a (001) plane. The helium atoms (black) are in their equilibrium positions but not all in the projection plane, white are nearest-neighbour atoms and grey next-nearest neighbours. Two next-nearest-neighbours in the centre of each figure are not shown.

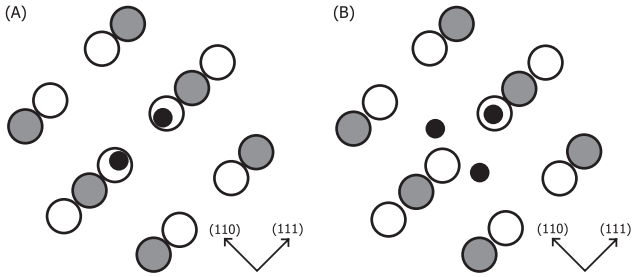

Figure 2. Projection of helium–vacancy clusters and fourteen neighbouring molybdenum atoms into a $(1\bar{1}0)$ plane. The helium atoms (black) are all in their equilibrium positions and positioned in the projection plane. White atoms are the eight nearest neighbours and grey the six next-nearest neighbours.

Table 1. Configurational factors used to calculate entropy contribution for the configurational entropy.

$W_{He_5V_1}$	48
$W_{He_4V_1}$	12
$W_{He_3V_1}$	24
$W_{He_2V_1}$	4
$W_{He_1V_1}$	1
W_V	1
W_{He}	6

has an equilibrium position in the centre of the unit cell, while the two helium atoms in the He_2V_1 cluster are positioned on a (111) line. For the cluster containing three helium atoms the equilibrium position of these atoms is on the $(1\bar{1}0)$ plane depicted in figure 2. The equilibrium position of helium atoms in the He_4V_1 cluster is in the form of a tetrahedron, and in the case of the He_5V_1 clusters the configuration can be described as a tetrahedron with one helium atom on the side.

The binding energies ΔE and $\tilde{\nu}$ were calculated as described above and can be found in table 3 together with experimentally determined values from the literature. Using these values the ODE system of equation (5) was solved for each set of parameters in the table and these results were used to calculate desorption spectra, both for the two sets of experimental data and for the calculations of this work. These spectra are depicted in figure 3 for a heating rate of 10 K s^{-1}. Also, the actual state evolution was calculated and can be found in figure 4. When interpreting these figures it is important to bear in mind that the experimental curves are not a

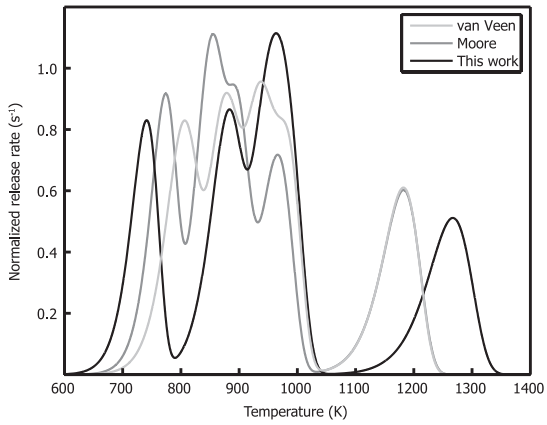

Figure 3. Helium release rates normalized to the initial value divided by 10 000 for a heating rate of $\beta = 10$ K s^{-1}, results for experimental parameters from [11] and [12] and this work. It is possible to resolve peaks for each of the five transitions in each case except for the $He_3V_1 \rightarrow He + He_2V_1$ and $He_2V_1 \rightarrow He + He_1V_1$ in our theoretical spectra since those are overlapping each other.

Table 2. Calculated formation energies for the vacancy state, the di-vacancy cluster and the two stable helium interstitial positions.

State	Formation energy (eV)	Reference [25]
V	2.61	3.0, 3.20, 3.24
V_2	5.43	
I_{tet}	5.28	
I_{oct}	5.45	

reproduction of the experimental results themselves but rather solutions achieved from modelling efforts with experimentally determined parameters as input.

5. Discussion

The calculated binding energies are in all but one case lower than the experimentally determined ones. This could be explained by the existence of a migration barrier at the helium–molybdenum interface not included in the calculations. However, the differences are in most cases smaller than the deviation between the two experimental series. The calculated frequencies differ more significantly from the experimentally determined ones, especially in the case of He_1V_1 where the

Table 3. Binding energy and effective frequency for the reaction $He_iV_j \rightarrow He + He_{i-1}V_j$.

	ΔE (eV)			$\tilde{\nu}$ (s^{-1})		
State	This work	Reference [11]	Reference [12]	This work	Reference [11]	Reference [12]
He_5V_1	2.00	2.11	2.32	1.9×10^{13}	0.7×10^{13}	6.2×10^{14}
He_4V_1	2.54	2.4	2.7	1.6×10^{14}	3×10^{13}	5.3×10^{15}
He_3V_1	2.54	2.6	2.61	2.3×10^{13}	5×10^{13}	2.3×10^{14}
He_2V_1	2.67	2.9	2.80	1.9×10^{13}	3.0×10^{14}	1.4×10^{14}
He_1V_1	3.64	3.8	3.75	7.6×10^{13}	5.0×10^{15}	3.0×10^{15}
He_2V_2	3.94	—	—	—	—	—
He_1V_2	3.90	—	—	—	—	—

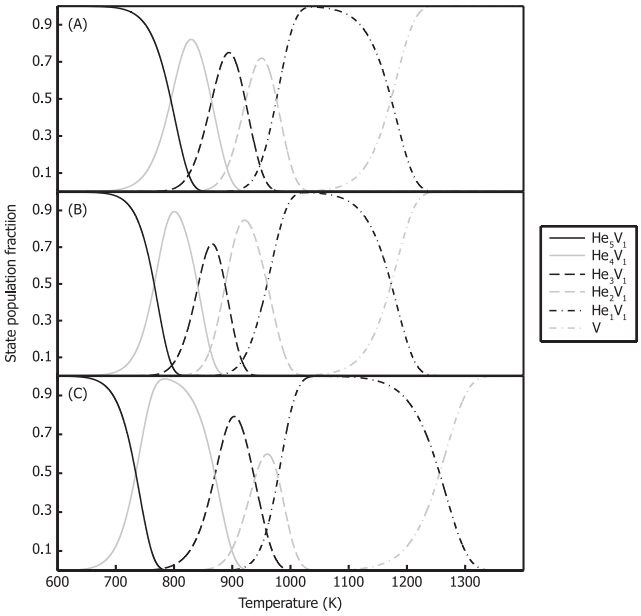

Figure 4. Modelling of state evolution with heating rate $\beta = 10$ K s^{-1}: (A) with experimental parameters from [11], (B) with experimental parameters from [12] and (C) *ab initio* data from this work.

difference is almost two orders of magnitude. One explanation for this could be a large change in entropy not considered in this work.

The reference experimental data in table 3 are based on helium desorption spectra. When considering the experimental observations in figure 3 together with the theoretical results it is important to remember that the depicted release rate is the sum of all transitions occurring at that moment in time (here related to a specific temperature through the constant heating rate). It is therefore possible to give more than one interpretation to such a spectrum, and the decomposition of the spectrum into the state evolutions in figure 4 is not guaranteed to have one single solution due to the nonlinearity of the jump rate in equation (4). This is not the case for the theoretical results since these are derived directly from calculated jump rates, and therefore give a unique state evolution resulting in a desorption spectrum.

One could anticipate the contribution of helium dissolution from other clusters containing more than one vacancy. However, under the current experimental conditions, such contributions are unlikely. First, the experiments which are reproduced here were conducted under controlled conditions where only thermal vacancies exist in the crystals. The implantation of helium was then performed with ions having less kinetic energy than the displacement energy of the molybdenum crystal to avoid radiation damage and thereby increased vacancy concentrations. The samples were then annealed to avoid oversaturation of vacancies and clustering of them [11, 12]. The unlikelihood of having di-vacancies at thermal equilibrium is also visible when comparing the numbers presented in table 2 since the formation energy of a di-vacancy is more than twice the formation energy of a mono-vacancy. Second, as shown in table 3, the binding energies of He_iV_2 clusters are significantly larger than those of the He_iV_1 clusters. This indicates that if those clusters would, in fact, be present in the crystal they would be visible as peaks at elevated temperatures in the desorption spectra: however, no authors report such peaks in their experimental spectra [11, 12].

In most of the studied helium–vacancy clusters the molybdenum atoms close to the cluster are significantly displaced from their equilibrium positions. This causes stress in the crystal and thereby an increase of the energy from elastic energy contributions. With periodic boundary conditions used in the calculations, the radial displacements from mirror images could affect the final results if the cell size is too small. To ensure the convergence with regard to cell size in these calculations the radial displacements, $u(r)$, of molybdenum atoms for the largest cluster were studied. These are depicted in figure 5 together with a fit of a theoretical prediction of these results and the strain that can be derived from these displacements. From linear elastic theory it can be concluded that the displacements will vary as [22, 23]

$$u(r) = A_1 r + \frac{A_2}{r^2} \tag{8}$$

with r as the distance from the centre of the defect cluster. Differentiating equation (8) gives the strain in the system. In linear elastic theory the elastic energy from, for example, a defect cluster is independent of system size. The calculations can therefore be assumed to be converged with respect to system size if the atoms close to the boundary of the supercell obey the predictions from linear elastic theory. As seen in figure 5 the atoms close to the cluster are displaced more than predicted by elastic theory. However, closer to the border of the supercell (1.75–3.5 lattice parameters) the atoms obey the conditions of elastic theory and strains are well below 1%,

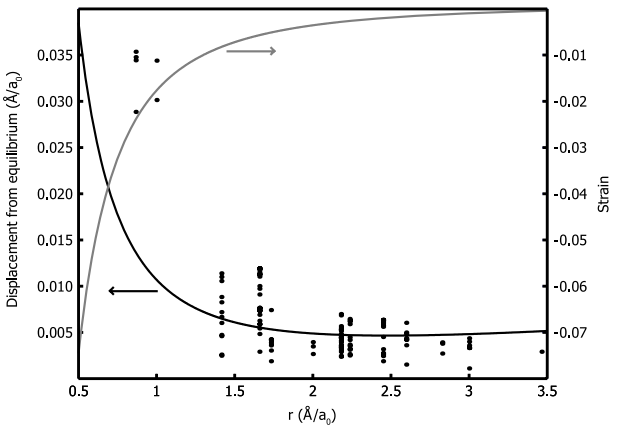

Figure 5. The displacement of each molybdenum atom in a supercell containing an He_5V_1 cluster and the stresses in the crystal due to this. The solid black line is the theoretical displacements; for details see the text. All lengths are normalized to the lattice parameter.

which means that the calculated energies are convergent with respect to cell size.

As seen in figures 3 and 4, experimental emission rates and state transitions are well reproduced for most of the transitions with the calculated parameters. However, in the low temperature as well as in the high temperature end of the spectrum, significant deviations are seen. In the low temperature regime, the transition from He_5V_1 to He_4V_1 is calculated to occur at lower temperatures than in experiments. This could be due to the existence of several configurations of the He_5V_1 cluster, all minimizing the total energy. If this would be the case the configurational entropy contribution to $\tilde{\nu}$ would be larger, increasing this frequency by a factor identical to the number of configurations. However, it is worth noticing that this is also the transition where the two experimental series differ the most.

The difficulty to model the He_1V_1 to V transition in the high temperature end can be attributed to several factors. First, the error associated with the exchange correlation functional [20, 21] is most pronounced in the transition from a molybdenum–helium to a molybdenum–vacuum surface. Second, the effective frequency calculated is much lower than the experimentally determined one. This could be due to entropy factors disregarded in this work. The explanation for the discrepancy could also come from a modelling error since the experimental work justifying the model was performed at 300 K [13], at which temperature the molybdenum atoms are practically immobile. However, at the temperatures of the He_1V_1 to V transition, typically above 1100 K the molybdenum self-diffusion could be a contributing factor [24], resulting in substitutional diffusion paths in the crystal.

When comparing the binding energies in table 3 with those calculated for helium–vacancy clusters in iron [2] one observes a common trend for both metals; the binding energy is a decreasing function when the number of atoms in the cluster increases. This indicates a similarity among the bcc metals regarding helium cluster dissolution, which could be anticipated for the inert gas helium dissolved in metals with the same crystal structure.

6. Conclusions

The current model of helium desorption, which is based on first-principles data, gives a good representation of experimentally observed desorption spectra: however, the He_1V_1 to V transition temperature is overestimated. This is most likely attributed to modelling errors. The foundation of the model assumed by previous authors [11, 12] is experimental work carried out at room temperature [13]. However, the He_1V_1 to V transition occurs at much higher temperatures where self-diffusion in molybdenum could allow for other, more complicated diffusion paths than the interstitial one.

References

[1] Ullmaier H 1993 Helium in metals *Landolt–Börnstein New Series* vol III/25 (Berlin: Springer) pp 380–435
[2] Fu C-C and Willaime F 2005 *Ab initio* study of helium in α-Fe: dissolution, migration, and clustering with vacancies *Phys. Rev.* B **72** 064117
[3] Seletskaia T, Osetsky Y, Stoller R E and Stocks G M 2005 Magnetic interactions influence the properties of helium defects in iron *Phys. Rev. Lett.* **94** 046403
[4] Seletskaia T, Osetsky Yu N, Stoller R E and Stocks G M 2006 Calculation of helium defect clustering properties in iron using a multi-scale approach *J. Nucl. Mater.* **351** 109–18
[5] Ventelon L, Wirth B and Domain C 2006 Helium-self-interstitial atom interaction in α-iron *J. Nucl. Mater.* **351** 119–32
[6] Fu C-C and Willaime F 2007 Interaction between helium and self-defects in α-iron from first principles *J. Nucl. Mater.* **367–370** 244–50
[7] Henriksson K O E, Nordlund K, Krasheninnikov A and Keinonen J 2005 Difference in formation of hydrogen and helium clusters in tungsten *Appl. Phys. Lett.* **87** 163113
[8] Henriksson K O E, Nordlund K, Krasheninnikov A and Keinonen J 2006 The depths of hydrogen and helium bubbles in tungsten: a comparison *Fusion Sci. Technol.* **50** 43–57
[9] Becquart C S and Domain C 2006 Migration energy of He in W revisited by *ab initio* calculations *Phys. Rev. Lett.* **97** 196402
[10] Becquart C S and Domain C 2007 *Ab initio* calculations about intrinsic point defects and He in W *Nucl. Instrum. Methods* B **255** 23–6
[11] van Veen A, Evans J H, Buters W TH M and Caspers L M 1983 Precipitation in low energy helium irradiated molybdenum *Radiat. Eff.* **78** 53–66
[12] Moore W T and Kornelsen E V 1985 Activation energies and frequency factors for the thermal desorption of he bound at vacancies in Mo *Radiat. Eff.* **90** 141–7
[13] Evans J H, van Veen A and Caspers L M 1983 The application of tem to the study of helium cluster nucleation and growth in molybdenum at 300 K *Radiat. Eff.* **78** 105–20
[14] Vineyard G H 1957 Frequency factors and isotope effects in solid state rate processes *J. Phys. Chem. Solids* **3** 121–7
[15] Ashcroft N W and Mermin N D 1976 *Solid State Physics* 1st edn (London: Harcourt College Publishers)
[16] Kresse G and Furthmüller J 1996 Efficient iterative schemes for *ab initio* total-energy calculations using a plane-wave basis set *Phys. Rev.* B **54** 11169
[17] Kresse G and Furthmüller J 1996 Efficiency of *ab initio* total energy calculations for metals and semiconductors using a plane-wave basis set *Comput. Mater. Sci.* **6** 15–50
[18] Kresse G and Joubert D 1999 From ultrasoft pseudopotentials to the projector augmented-wave method *Phys. Rev.* B **59** 1758

[19] Makov G and Payne M C 1995 Periodic boundary conditions in *ab initio* calculations *Phys. Rev.* B **51** 4014–22
[20] Mattsson A E and Kohn W 2001 An energy functional for surfaces *J. Chem. Phys.* **115** 3441–3
[21] Mattsson T R and Mattsson A E 2002 Calculating the vacancy formation energy in metals: Pt, Pd, and Mo *Phys. Rev.* B **66** 214110
[22] Eshelby J D 1954 Distortion of a crystal by point imperfections *J. Appl. Phys.* **25** 255
[23] Christian J W 1975 *The Theory of Transformations in Metals and Alloys, Part I, Equilibrium and General Kinetic Theory* 2nd edn (Oxford: Pergamon)
[24] Maier K, Mehrer H and Rein G 1979 Self-diffusion in molybdenum *Z. Metallk.* **70** 271–6
[25] Schultz H 1993 *Landolt–Börnstein New Series* vol III/25 (Berlin: Springer) pp 140–6